IOPscience iopscience.iop.org

Home Search Collections Journals About Contact us My IOPscience

Correlations in the electronic properties of AlCuFe quasicrystals and high-order approximants: ^{57}Fe Mössbauer, and ^{27}Al and ^{65}Cu nuclear magnetic resonance studies

This article has been downloaded from IOPscience. Please scroll down to see the full text article.

1999 J. Phys.: Condens. Matter 11 7523

(http://iopscience.iop.org/0953-8984/11/39/309)

View the table of contents for this issue, or go to the journal homepage for more

Download details:
IP Address: 171.66.16.220
The article was downloaded on 15/05/2010 at 17:30

Please note that terms and conditions apply.

J. Phys.: Condens. Matter **11** (1999) 7523–7543. Printed in the UK PII: S0953-8984(99)03503-1

Correlations in the electronic properties of AlCuFe quasicrystals and high-order approximants: ^{57}Fe Mössbauer, and ^{27}Al and ^{65}Cu nuclear magnetic resonance studies

R A Brand†, J Pelloth†, F Hippert‡ and Y Calvayrac§

† Department of Physics, Gerhard-Mercator-Universität GH Duisburg, D-47048 Duisburg, Germany

‡ Laboratoire de Physique des Solides, associé au CNRS, Bâtiment 510, Université de Paris Sud, F-91405 Orsay Cédex, France

§ CECM/CNRS, 15 rue G Urbain, F-94407 Vitry Cédex, France

Received 16 April 1999

Abstract. We have investigated the local electronic properties and the atomic order in the $Al_{100-x-y}Cu_xFe_y$ phases using ^{57}Fe Mössbauer as well as ^{27}Al and ^{65}Cu nuclear magnetic resonance (NMR) spectroscopies. We have studied samples along the existence domains of the icosahedral quasicrystalline (i-) and the high-order approximant phases, given by two close-lying parallel lines in the concentration diagram. In addition, we have also studied a series of intermediate concentrations situated between these lines and retained in a *metastable* i-phase by quenching. It is found that the ^{57}Fe Mössbauer centre shift (isomer shift) and quadrupole splitting are linearly correlated with each other over the range of compositions and structures for all samples, which reveals systematic changes in the orbital occupations on Fe atoms with composition. In addition, it is found that the ^{27}Al NMR average electronic shift follows this correlation. The results are discussed in terms of the hybridization of iron d states with the p and induced d states of Al. We have studied also a low-order cubic approximant phase containing Si as well as several non-approximant crystalline phases.

1. Introduction

The discovery of icosahedral point symmetry in an AlMn alloy by Shechtman *et al* [1] prompted intensive research which has now been continuing for more than ten years on the structure, chemical order, and electronic properties of these new materials [2–4]. The introduction of the cut-and-project method now allows us to construct quasiperiodic lattices which yield the correct experimental diffraction line positions [5]. However, the problem of the atomic decoration (chemical order) on such a lattice remains only partially solved [6–8]. Many different systems have been found which form quasicrystalline structures, some of which are stable phases. These are always confined to narrow composition ranges. Many of the physical properties of the stable quasicrystals are atypical for metals. They exhibit very low thermal conductivity, as well as a reduced density of electronic states at the Fermi level E_F and anomalous transport properties (very high electrical resistivity with a negative temperature coefficient) reminiscent of those of non-metals (see for example [9–11]). The origin of the stability of these structures as well as the relation to these atypical electronic properties is a controversial issue. A Hume-Rothery type of electronic phase [12] would lead naturally to a connection between the phase composition and the stability, as well as to a reduced density of states at E_F [9, 10].

0953-8984/99/397523+21$30.00 © 1999 IOP Publishing Ltd

We have therefore undertaken a systematic study of the local electronic properties and atomic order in the quasicrystalline and approximant phases of $Al_{100-x-y}Cu_xFe_y$ in order to investigate this question. This ternary alloy system builds a stable icosahedral quasicrystalline phase and several approximant phases in a very small concentration range [13]. Here and in the following, the Cu (x) and Fe (y) concentrations in at.% are given as (x, y). At 700 °C the icosahedral (i-) phase occupies a small triangular domain, the corners of which are (23.7, 12.7), (24.4, 13.1), and (29.6, 10.5) [13]. At lower temperatures, the existence domain of the i-phase is reduced to a narrow elongated domain, which can nearly be approximated by a line segment given by $y = -0.4x + 22.7$ extending from (24.4, 12.9) to (26.0, 12.3), hereafter denoted as the I-line. For compositions along this line, long low-temperature annealings do not lead to any changes in the x-ray diffraction pattern, which suggests that the i-phase is the stable structure at low temperature. (Stable and metastable as used here will refer to the low-temperature stability.) Several periodic high-order approximant phases of the icosahedral AlCuFe phase, with pentagonal (p-, $p/q = 4/3$), rhombohedral (r-, $p/q = 3/2$) and orthorhombic (o-) symmetry, have also been identified, where p/q indicates the rational approximation to the golden ratio τ characterizing the approximant phase [13]. In the notation of reference [13], the p-phase is P1. For the o-phase, p/q depends on the spatial direction. At 700 °C, the existence domains of the p-, r-, and o-phases are also localized along a narrow strip extending from (23.3, 12.3) to (30.1, 9.6) which is moreover nearly parallel to that of the stable i-phase at low temperature and corresponds therefore to the same well-defined substitution law. Neglecting the small two-phased intervals between the three existence domains of the p-, r-, and o-phases and the lateral extension in the Fe concentration, this strip can be approximated by the line segment $y = -0.4x + 21.6$ with the limits above, hereafter denoted as the A-line. At lower temperatures, only the rhombohedral phase is stable. Intermediate annealings and quenching are used to retain the metastable p- and o-phases to room temperature. All of these approximant alloys can also be prepared in a metastable icosahedral state.

The different high-order approximant phases are structurally related to the icosahedral quasicrystalline one by a six-dimensional shearing transformation linking the different diffraction lines in their respective x-ray spectra [13]. Thus we expect very similar local chemical and electronic structures among these phases. The fact that the existence domains at lower temperatures practically reduce to lines with little lateral extent implies in addition a very strict substitution rule: five Cu atoms are substituted for with three Al and two Fe atoms. This is similar to the case of a pseudo-binary substitution between two isostructural end-points. But the current structural and decoration models give no justification for the existence of two different lines in the composition diagram.

In the usual Hume-Rothery compounds [12], the crystal structure is stabilized by an effective interaction between the Fermi surface and the Brillouin–Jones zone (BZ) due to electron scattering on the lattice planes. The matching determines the number of conduction electrons per atom e/a. This model has often been applied to quasicrystals and their high-order approximants to interpret their stability. In fact, in the case of $Al_{100-x-y}Cu_xFe_y$, the substitution rule given above corresponds to a constant value of e/a (1.865 for the I-line and 1.92 for the A-line) assuming usual valences for Al, Cu, and Fe atoms ($v_{Al} = 3$, $v_{Cu} = 1$, $v_{Fe} = -2$) [10,14]. However, this model is too rough to justify two different stability domains.

From the above, it is clear that it is necessary to study the local chemical and electronic structure along these two composition lines for stable structures. This may bring to light the link between the electronic properties and the phase stability. We have undertaken a systematic study combining ^{57}Fe Mössbauer, as well as ^{27}Al and ^{65}Cu nuclear magnetic resonance (NMR) spectroscopies [15,16]. In the present paper, we will focus on the correlations between several of the different hyperfine properties and the implications for the local structure. We will

summarize the influence of long-range order at a given composition and that of changes in composition. We will then establish that there exists a correlation in the ^{57}Fe average centre shift and quadrupole splitting as well as the ^{27}Al average electronic shift for all icosahedral and high-order approximant samples. These results will be compared to those for the cubic low-order approximant [17], as well as non-approximant phases.

2. Samples studied

All of the samples used were prepared at CECM by planar-flow casting methods. They have been annealed in order to eliminate the disorder and the small amount of the cubic (B2) β-phase (a volume fraction of the order of a few %) usually present in the as-quenched samples. Sample compositions are given in table 1. Samples previously studied in references [15, 16] have been chosen to span the existence domains of the icosahedral quasicrystalline (I-line) and high-order approximant (A-line) phases. Samples with compositions along the A-line have been prepared in the different stable (r-) and metastable (p-, o-, and i-) states at the same composition by using different heat treatments and quenchings [15, 16]. The compositions studied, as well as the existence domains of the i-, p-, r-, and o-phases at 700 °C from reference [13], have been drawn in figure 1.

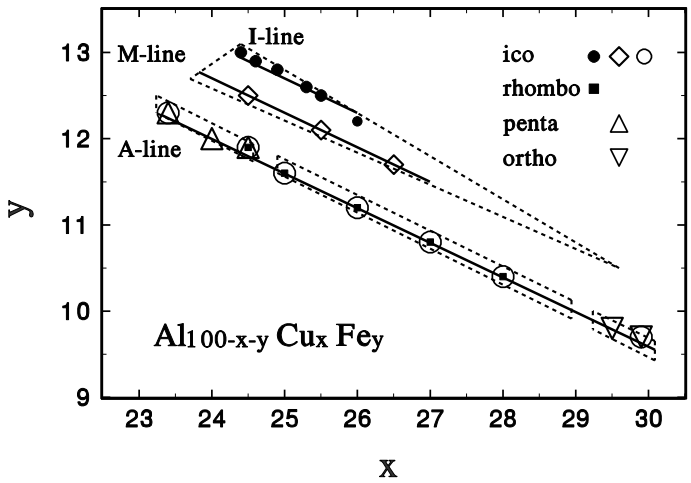

Figure 1. A concentration diagram showing the samples studied here. The boundaries of the stability domains of the 'ico' (icosahedral), 'penta' (pentagonal), 'rhombo' (rhombohedral), and 'ortho' (orthorhombic) phases at 700 °C from [13] have been drawn as dotted lines. Samples in structures which are stable at low temperature are represented by full symbols. Shown as well are the I-, A-, and M-lines as explained in the text.

Three samples belonging to the single-phase icosahedral domain at 700 °C have been chosen along a line parallel to the I- and A-lines, i.e. with the same substitution law. This line segment, hereafter denoted as the M-line, is given by $y = -0.4x + 22.3$ and extends from $x = 23.8$ to $x = 27$. For such samples the i-phase is not stable at room temperature but a metastable (and defective) i-phase is retained by quenching from 700 °C. In a Hume-Rothery approach, described in the introduction, this M-line is a line of constant $e/a = 1.885$. However, one must emphasize that, in contrast to the I- and A-lines, this M-line has no particular physical meaning. Any other parallel line, in between the I- and M-lines and within the single-phase icosahedral domain at 700 °C, would connect samples obeying the very same substitution

Table 1. Samples studied including the line (I-, A-, or M-) and long-range order, the Cu and Fe concentrations (x, y), and the lattice parameters a_{6D} for icosahedral samples. Stable and metastable refer to stability at low temperature. Phases are indicated as 'ico' (icosahedral), 'penta' (pentagonal), 'rhombo' (rhombohedral), and 'ortho' (orthorhombic). Also included are the ^{57}Fe average centre shift $\langle\delta\rangle$ and quadrupole splitting $\langle\Delta\rangle$, and the ^{27}Al average frequency shift $\langle\delta\nu\rangle_{\mathrm{Al}}$. The error bars are ± 0.02 mm s^{-1} on $\langle\delta\rangle$ and $\langle\Delta\rangle$; ± 0.3 kHz on $\langle\delta\nu\rangle_{\mathrm{Al}}$.

Line and state	Sample (x, y)	a_{6D} (Å)	$\langle\delta\rangle$ (mm s^{-1})	$\langle\Delta\rangle$ (mm s^{-1})	$\langle\delta\nu\rangle_{\mathrm{Al}}$ (kHz)
I-line:	i-(24.4, 13.0)	6.3198	0.241	0.368	−0.1
stable ico	i-(24.6, 12.9)	6.3193	0.240	0.372	0.6
	i-(24.9, 12.8)	6.3180	0.240	0.372	0.8
	i-(25.3, 12.6)	6.3173	0.238	0.374	1.6
	i-(25.5, 12.5)	6.3176	0.237	0.379	2.0
A-line:	i-(23.4, 12.3)	6.3181	0.218	0.409	4.5
metastable ico	i-(24.5, 11.9)	6.3168	0.219	0.415	5.1
	i-(25.0, 11.6)	6.3149	0.216	0.422	5.5
	i-(26.0, 11.2)	6.3125	0.217	0.431	—
	i-(27.0, 10.8)	6.3108	0.214	0.435	6.7
	i-(28.0, 10.4)	6.3088	0.211	0.435	—
	i-(29.9, 9.7)	6.3042	0.210	0.437	9.4
A-line:	r-(24.5, 11.9)	—	0.219	0.411	5.1
stable rhombo	r-(25.0, 11.6)	—	0.217	0.420	—
	r-(26.0, 11.2)	—	0.213	0.436	5.9
	r-(27.0, 10.8)	—	0.215	0.432	—
	r-(28.0, 10.4)	—	0.212	0.436	7.4
A-line:	p-(23.4, 12.3)	—	0.229	0.420	4.9
metastable penta	p-(24.0, 12.0)	—	0.228	0.418	5.5
	p-(24.5, 11.9)	—	0.223	0.412	5.1
A-line	o-(29.5, 9.8)	—	0.211	0.438	8.3
metastable ortho	o-(29.9, 9.7)	—	0.208	0.437	8.9
M-line:	i-(24.5, 12.5)	6.3158	0.229	0.392	3.3
metastable ico	i-(25.5, 12.1)	6.3149	0.227	0.395	3.3
	i-(26.5, 11.7)	6.3139	0.226	0.400	3.8
Metastable ico	i-(26.0, 12.2)	6.3153	0.2337	0.3831	2.0
Cubic approximant 7% Si	c-(25.5, 12.5)	—	0.217	0.337	7.6
Crystalline	β-(25.0, 25.0)	—	0.331	0.248	—
non-approximants	ω-(20.0, 10.0)	—	0.143	0.0	—
	λ-(0.0, 23.0)	—	(1) 0.21	0.0	—
			(2) 0.20	0.41	

law with a different constant value of e/a. The M-line has been chosen at the limit of the single-phase icosahedral domain at 700 °C in order to get the maximum possible composition changes with respect to samples along the I-line, as can be seen in figure 1. We have also studied another metastable icosahedral phase, i-(26, 12.2), in between the I- and M-lines.

In addition, a low-order cubic (c-, $p/q = 1/1$) approximant phase has been studied: $Al_{55}Cu_{25.5}Fe_{12.5}Si_7$ where 7% Si has been substituted for Al [17]. Several crystalline phases

with compositions near the quasicrystalline and high-order approximant phases have been studied as well. These are the B2 cubic phase denoted as β, a tetragonal phase denoted as ω [18], and a monoclinic phase denoted as λ [19]. The ternary β-phase is isomorphous to the binary B2 AlFe phase. The complex λ-phase (102 atoms/cell) is isomorphous to $Al_{13}Co_4$ which is an approximant to the AlCuCo decagonal phase.

3. Hyperfine properties at the Fe sites

3.1. Analysis of ^{57}Fe Mössbauer spectra

Typical ^{57}Fe Mössbauer spectra for one stable icosahedral phase and one metastable high-order approximant phase are shown in figures 2(a) and 2(b). (Spectra from the M-line samples are similar.) The 1/1 cubic approximant is shown in figure 2(c). All of these spectra show evidence for a broad distribution of centre shift (isomer shift) δ as well as the quadrupole splitting Δ due to electric field gradients (EFG). The distributions have been approximated using a Gaussian form (Voigt lineform) and evaluated using the exact transmission integral. The fitting method has been discussed in more detail in reference [15]. We report here the average values $\langle\delta\rangle$ and $\langle\Delta\rangle$ in table 1. In addition, we have also used the Gaussian isotropic model (GIM) distribution [20] (but without a transmission integral). Slightly different average values of the hyperfine parameters are found, but the same systematic trends are obtained. The ^{57}Fe Mössbauer spectra for the crystalline phases are given in figures 2(d) to 2(f). In the tetragonal ω-phase, the quadrupole splitting is very low, although the structure is not cubic. The quadrupole splitting seen for the cubic β-phase is solely due to chemical disorder. In

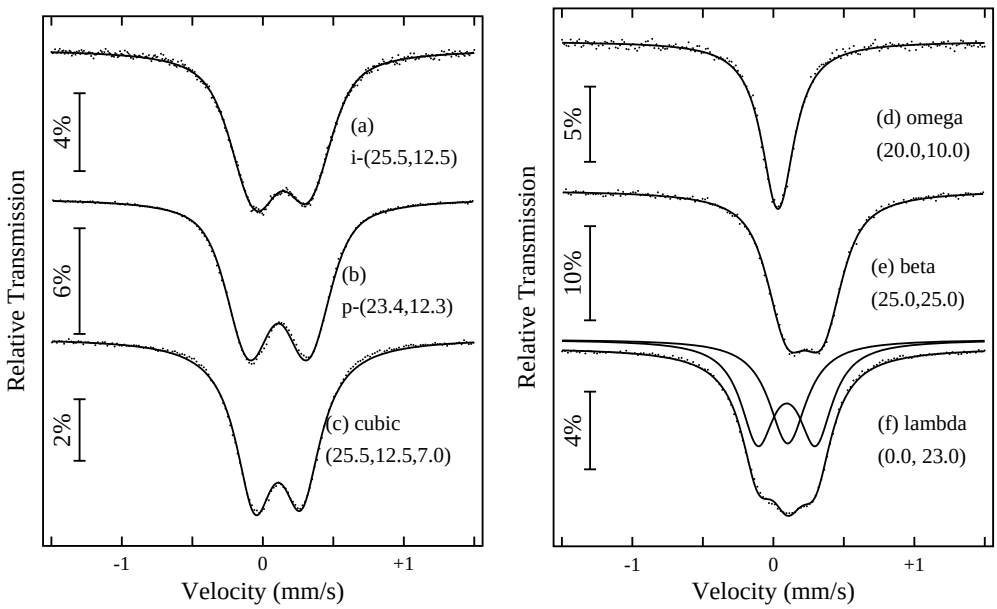

Figure 2. Typical Mössbauer results for the (left) stable icosahedral i-(25.5, 12.5), metastable pentagonal p-(23.4, 12.3), and low-order cubic approximant c-(25.5, 12.5) with 7 at.% Si, and (right) the crystalline non-approximant ω-, β-, and λ-samples at room temperature. For the λ-phase spectrum, the (1) single-line and (2) quadrupole doublet subspectra are discussed in the text. All spectra have been fitted with a transmission integral (solid line).

the case of the λ-phase, the fit of either a quadrupole distribution or of two subspectra led to two distinct subspectra with roughly (1) about one third of the weight in a single line (or small EFG), and (2) two thirds in a quadrupole doublet. This could correspond to (a) the eight Fe5 atoms and (b) four of each of the Fe1 to Fe4 atoms in the monoclinic unit cell given by Black [19]. However, the weight of subspectrum (1) relative to that of (2) in the fit is sensitive to the EFG splitting permitted for subspectrum (1), so this is only a suggestion, and we have shown the fit for $\Delta(1) = 0$. (See the second article by Black for a discussion of iron site environments. See Faudot [21] as well as Freiburg and Grushko [22] for a discussion of the complicated λ-phase.) The spectra for the crystalline phases differ strongly from those for the first three samples, both in average centre shift $\langle\delta\rangle$ and quadrupole splitting $\langle\Delta\rangle$. The slight asymmetry seen in the spectra for the icosahedral and approximant spectra is due to slight changes in isomer shift over the quadrupole splitting distribution. This will be ignored here (and has nothing to do with the correlation effects discussed in section 3.3). Only average values of δ and Δ will be used to characterize the hyperfine properties at the iron nucleus, and these are independent of this small effect.

3.2. Dependence on long-range order and composition

By comparing the results for identical compositions along the A-line but in different structures (the i-phase compared to r-, o-, and p-phases), we found in previous papers [15, 16] that *at a given composition* no differences in the ^{57}Fe hyperfine properties can be detected. The same conclusion was obtained for the local electronic properties and electrical field gradients at the Cu and Al sites probed by NMR. Therefore *the local electronic and atomic structures are insensitive to the nature of the long-range order* of the icosahedral and high-order approximants.

But we did detect systematic composition dependencies for the ^{57}Fe average centre shift $\langle\delta\rangle$ and quadrupole splitting $\langle\Delta\rangle$, as shown in figures 3(a) and 3(b) as functions of the Cu concentration x. (Similar results are observed as a function of Al or Fe concentration.) For all of the i-phases along the I-line, $\langle\delta\rangle$ and $\langle\Delta\rangle$ form one continuous slow variation. All of the quasicrystalline and approximant phases along the A-line form another continuous slow variation which is close to being parallel to the first. Much larger changes are observed when going from one domain to another, although the composition variations involved are much smaller than within each domain. The samples along the M-line also show similar properties, forming one continuous slow variation along a parallel line in between those for the I- and A-line samples, shown in figure 3. The same trends are observed when analysing the concentration dependence of the average shifts of the NMR ^{27}Al and ^{65}Cu lines (see [15, 16] and section 4.3). Therefore each hyperfine property depends on the composition, but different composition changes are far from being equivalent. Following the directions of the existence domains (five Cu atoms substituting for three Al and two Fe) induces *small* changes in properties, similar for all three lines presented here (I-, A-, and M-lines). Changes induced by composition variations perpendicular to these (for example approximately at constant Cu composition: see figure 1) are *much more rapid*. We conclude that the variations of $\langle\delta\rangle$ and $\langle\Delta\rangle$ with composition are due to changes in the electronic and quadrupole couplings at the Fe sites. It remains to be seen whether there is a hidden unity between these different lines, and the origin of the striking variations in the local electronic properties has yet to be understood.

3.3. Correlation in the ^{57}Fe hyperfine properties of icosahedral and high-order approximants

Indeed, the average centre shift $\langle\delta\rangle$ and the average quadrupole splitting $\langle\Delta\rangle$ at the ^{57}Fe nucleus are correlated for samples along the I-, M-, and A-lines. To show this, we have

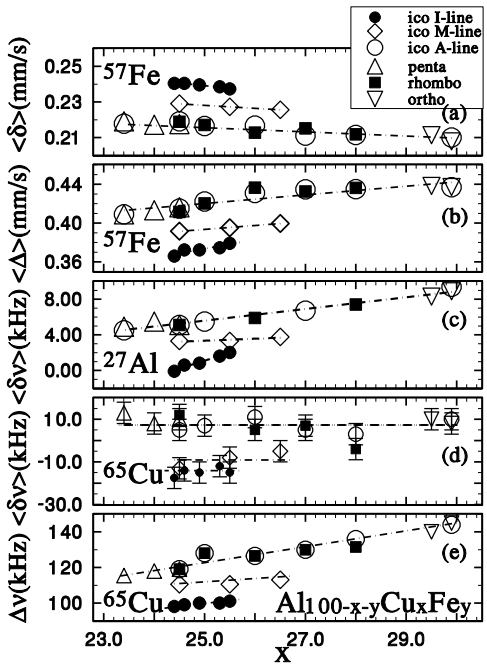

Figure 3. Composition and structural dependences for samples along the I-, the A-, and the M-lines. Shown are: the ^{57}Fe Mössbauer (a) average centre (isomer) shift $\langle\delta\rangle$ and (b) quadrupole splitting $\langle\Delta\rangle$; (c) ^{27}Al and (d) ^{65}Cu NMR central-line average frequency shifts $\langle\delta\nu\rangle$ in 6.9952 T; as well as (e) the ^{65}Cu NMR linewidth. The lines are guides to the eye.

plotted $\langle\Delta\rangle$ as a function of $\langle\delta\rangle$ in figure 4, for all of the i- and the high-order approximant phases (some preliminary results were published in [23]). It is remarkable that this figure shows clear evidence for a *single continuous* linear variation over *all* of these phases. From the concentration dependence (figure 3), it is to be expected that we find I-, A-, and M-line samples along three parallel line segments in figure 4. What is surprising is to find them *along the very same line*. This demonstrates that there is a strict correlation in changes of the hyperfine properties at the iron site extending over the whole range of compositions for these phases. We obtain from a linear fit

$$\langle\Delta\rangle = -2.23\langle\delta\rangle + 0.904 \text{ mm s}^{-1} \tag{1}$$

shown in figure 4 as the correlation line. The 95% confidence bounds are also shown. There is however little if any overlap in the line segments occupied by the results from the I-, A-, and M-line samples. This results from the large difference in concentration dependence of $\langle\delta\rangle$ and $\langle\Delta\rangle$ along, as compared to between, these lines.

In figure 5 we show these same samples compared to other phases presented here as well as some results from the literature. Shown is the result for the low-order 1/1 cubic approximant: this falls close to but definitely outside the confidence bounds of the correlation line. In addition, the crystalline λ-sample is shown. (The results for β and ω—see table 1—are not shown, as these crystalline samples fall far away from the correlation line.) In view of these results, we expect that for any single-phase icosahedral sample (stable or metastable) the hyperfine parameters $\langle\delta\rangle$ and $\langle\Delta\rangle$ will fall on the correlation line. Indeed this is the case for the metastable icosahedral sample i-(26, 12.2) found in between the I- and M-lines in the composition diagram, as is shown in figure 4.

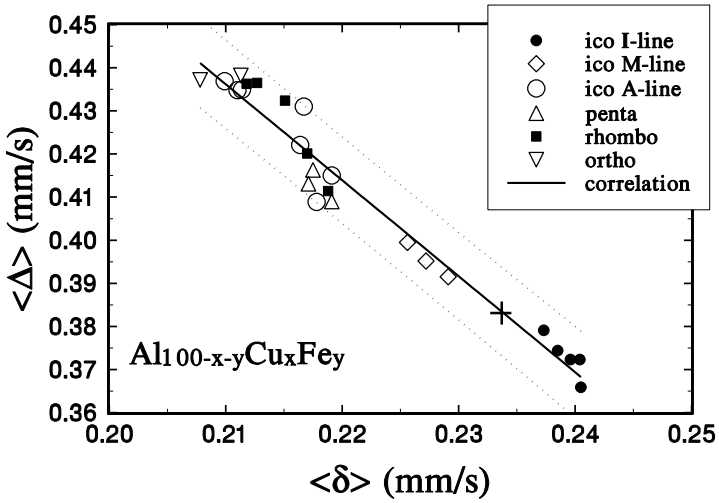

Figure 4. A correlation diagram showing the linear dependence between the ^{57}Fe Mössbauer $\langle\delta\rangle$ and $\langle\Delta\rangle$ parameters for samples along the I-, A-, and M-lines. The sample marked + is the additional i-phase i-(26.0, 12.2) discussed in the text. The solid line is a fit to the data and the dotted lines are the 95% confidence limits of the fit.

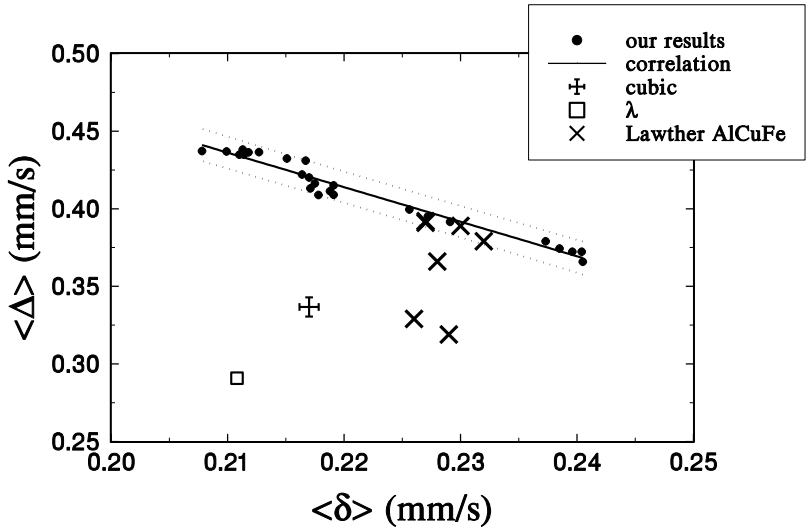

Figure 5. Our results (small solid dots) for the icosahedral quasicrystals and high-order approximants compared with results for the 1/1 cubic low-order approximant sample, and the crystalline λ-phase. The correlation line and confidence bounds are taken from figure 4. Data on samples from Lawther and Dunlap [24] are shown as well. Only their samples with compositions near our A-line fall within the confidence bounds.

Lawther and Dunlap [24] have presented Mössbauer hyperfine studies of AlCuFe for several different compositions and heat treatments. Their results are also shown in figure 5. Their sample compositions i-(25, 12) and i-(25, 12.5) lie between the I- and A-lines. For these two samples, their results lie very near ours for our M-line samples, as we would expect. They

have also reported on (20, 15) samples with different heat treatments. These results lie far from the correlation line, as is also shown in the figure. However, the (20, 15) composition, although on the extension to the I-line, is now known to lie in a multiphase region of the phase diagram [13]. We can also compare these results with published data for Fe–Al binary compounds, the ordered binary phases B2 β-FeAl ($\delta = 0.26$, $\Delta = 0$ mm s^{-1}) [25], as well as Fe_2Al_5 ($\delta = 0.23$, $\Delta = 0$ mm s^{-1}) [25]. The hyperfine results for these two compounds also fall far away from the correlation line. We conclude that the correlation line found here for the icosahedral quasicrystalline and high-order approximant phases is a *unique feature* of these phases and reflects their *local chemical and electronic structure.*

Thus the question arises of whether the hyperfine properties at the ^{27}Al and ^{65}Cu sites vary in a systematic way with respect to those of ^{57}Fe. This is the subject of the following section.

4. Hyperfine properties at the Al and Cu sites

4.1. Analysis of the ^{27}Al and ^{65}Cu NMR spectra in high field

For the icosahedral, high-order approximant phases, the ^{27}Al and ^{65}Cu NMR spectra in high magnetic field ($\sim$7 T) consist of two parts. There is a narrow central line associated with the $m = -1/2, m = +1/2$ nuclear spin transition. On this is superposed a much broader line from the first-order quadrupole splitting of the remaining Al and Cu nuclear transitions [15–17, 26]. The absence of any resolved feature in either of these two parts indicates a broad distribution of electric field gradients (EFG) and hence of local environments at both the Al and Cu sites. All samples have been studied in fixed magnetic field ($B = 6.9952$ T) by changing the frequency step by step and measuring the spin-echo integral. This method is not suitable for measuring broad lines because the detection circuit has to be re-tuned at each frequency. Thus at high field only the ^{27}Al and ^{65}Cu central lines were measured. (The ^{63}Cu central line was not studied because it is superposed on the large ^{27}Al first-order quadrupole line.) Typical results are shown in figure 6 for one stable I-line icosahedral phase and one A-line approximant phase. Results for the 1/1 cubic approximant are similar [17].

The frequency splitting of the $m = 1/2, m = -1/2$ transition depends on the interaction of the nuclear spin with the conduction electrons H_e (a first-order effect) and on quadrupole couplings H_q (a second-order effect). It depends moreover on the orientation of the magnetic field with respect to the local symmetry axis. The shape of the central line results from the distribution of the resonance frequencies and reflects both the powder average and the distribution of the electronic and quadrupole coupling parameters. No meaningful fit of the central lines measured in 7 T can be obtained because of the large number of parameters. Fits in lower field, where quadrupole effects (proportional to $1/B$) dominate, are possible (see the appendix). Thus we have only calculated the average frequencies $\langle\nu\rangle$ of the central lines measured in high field (after subtracting the contribution of the first-order quadrupole lines [27]) and obtained the average frequency shift $\langle\delta\nu\rangle = \langle\nu\rangle - \nu_L$. Here $\nu_L = \gamma_n B$ is the reference (Larmor) frequency in the applied field (77.6047 MHz for ^{27}Al with $\gamma_n = 11.094$ MHz T^{-1} and 84.565 MHz for ^{65}Cu with $\gamma_n = 12.089$ MHz T^{-1}). The error bars on $\langle\delta\nu\rangle$ are $\pm$0.3 kHz for the ^{27}Al and $\pm$5 kHz for the ^{65}Cu central lines. This does not include the uncertainty on ν_L which simply leads to an overall shift of the data. The $\langle\delta\nu\rangle$ value for the ^{65}Cu central line is very sensitive to the estimation of the background which causes the large error bar quoted above.

The average frequency shifts $\langle\delta\nu\rangle$ of both Al and Cu lines exhibit clear composition dependencies as will be described in sections 4.3.1 and 4.3.2. However, it should be emphasized that they are the sum of electronic and quadrupole shifts which could both depend *a priori* on composition. Second-order quadrupole couplings contribute to an average negative shift of the

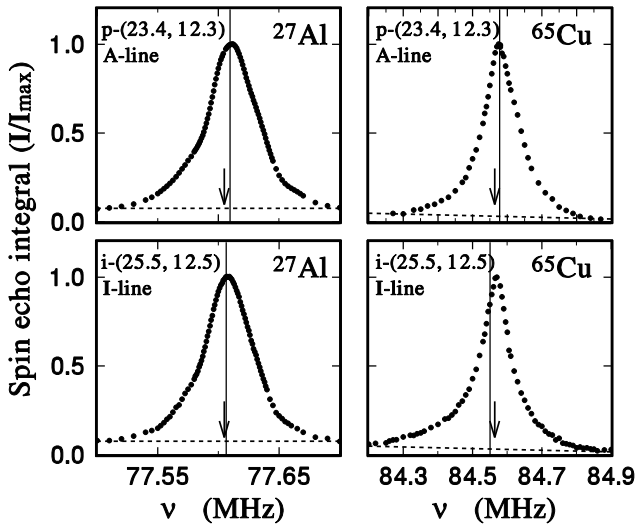

Figure 6. Typical ^{27}Al and ^{65}Cu NMR central lines measured in a fixed field (6.9952 T). The spin-echo integral has been measured as a function of frequency. The arrows indicate the reference frequencies $\nu_L = 77.6047$ MHz for the ^{27}Al and $\nu_L = 84.565$ MHz for the ^{65}Cu resonance. Average frequencies are shown by the thin solid lines. The dashed lines indicate the contributions of the other nuclear transitions (first-order quadrupole).

line $\langle \delta\nu_q \rangle$ inversely proportional to the applied field, while the average shift due to electronic couplings $\langle \delta\nu_e \rangle$ is proportional to the applied field. Experiments in different fields are then required to separate these two contributions.

4.2. Separation of quadrupole and electronic contributions

We performed additional NMR experiments by using a field-sweep spectrometer where the spin-echo integral is measured as a function of the applied field at a fixed frequency ν_0. The complete NMR spectra, including the ^{27}Al, ^{63}Cu, and ^{65}Cu resonances, were measured at several frequencies in the range 18–40 MHz. (Since increasing field at fixed frequency corresponds to decreasing frequency at fixed field, the copper resonances are now to the left of the aluminium one.) In total, four samples were studied in this way at $T = 95$ K, one along the I-line: i-(25.5, 12.5), and three along the A-line: p-(23.4, 12.3), r-(26.0, 11.2), and o-(29.9, 9.7). The NMR spectra were found to be temperature independent, so these data can be compared with central lines measured at 300 K in a fixed field ($\approx$7 T).

4.2.1. ^{27}Al NMR spectra. The first-order quadrupole lines are found to be identical for the four samples studied within the experimental uncertainties. As an example, spectra recorded at $\nu_0 = 40.454$ MHz are shown in figure 7. As these samples span the concentration domain studied, it is reasonable to conclude that the first-order quadrupole couplings and hence *the EFG distributions at the Al sites are the same in all samples*. (The satellite lines are only affected by quadrupole couplings because in first perturbation order H_q is much larger than H_e in the samples studied.) Therefore the contribution of quadrupole couplings to the central line is sample independent and the variations of $\langle \delta\nu \rangle_{Al}$ in 7 T reported in table 1 are *only due to changes in the electronic couplings at the Al sites*. In order to obtain the average electronic frequency shift $\langle \delta\nu_e \rangle_{Al}$, one should then, in first approximation, subtract the constant (negative)

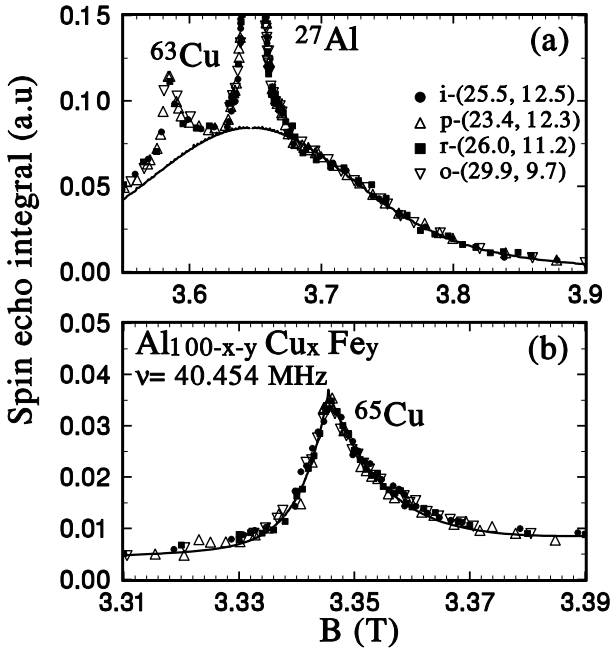

Figure 7. NMR field-sweep spectra measured at $\nu_0 = 40.454$ MHz for one icosahedral sample along the I-line (i-(25.5–12.5)) and three approximant samples along the A-line (p-(23.4, 12.3), r-(26.0, 11.2), and o-(29.9–9.7)): (a) ^{27}Al first-order quadrupole spectra and (b) ^{65}Cu central lines. (When comparing figures 6 and 7 one should remember that increasing field at fixed frequency corresponds to decreasing frequency at fixed field.) Solid lines are fits using the GIM model (see the appendix).

quadrupole average shift $\langle \delta\nu_q \rangle_{Al}$. The latter quantity can be deduced from fits of the central line measured at low frequency as explained in the appendix and is found to be equal to -11 kHz at 7 T.

4.2.2. ^{65}Cu NMR spectra. No accurate information can be obtained on the first-order ^{65}Cu NMR quadrupole spectrum which is mixed with the ^{27}Al one. Therefore only the ^{65}Cu central lines could be studied. The spectra measured at $\nu_0 = 40.454$ MHz in varying field for the four samples studied are found to be identical within the experimental accuracy (figure 7). On the other hand, at 7 T the linewidth of the ^{65}Cu central line varies significantly from sample to sample (see figure 3(e)). If this were mainly due to variations in the EFG at the Cu sites, then clear differences would have been detected in the field-sweep spectra at 40.454 MHz. However, from studies on sample i-(25.5, 12.50) at lower frequency, we have observed that the quadrupole contribution accounts for only $\sim$80% of the linewidth measured in 40.454 MHz. Therefore, small variations of the EFG from sample to sample, compensated by changes in the electronic couplings such that the total linewidth in 40.454 MHz remains constant, cannot be excluded [28]. In conclusion, the EFG distribution at the Cu sites does not vary strongly with composition and therefore the composition dependence of the average shift and linewidth of the ^{65}Cu central line in high field (7 T) are *mainly due to electronic effects*. From fits of the ^{65}Cu central line measured for sample i-(25.5, 12.5) at low frequency (see the appendix) we deduce that $\langle \delta\nu_q \rangle_{Cu}$ in 7 T is equal to -29 kHz for this sample (and assume similar values for all samples).

4.3. Composition dependence of the local electronic properties

4.3.1. Al sites. The composition dependence of the average frequency shifts of the ^{27}Al central lines in 7 T is summarized in figure 3(c) as a function of the Cu concentration. The overall variation of $\langle\delta\nu\rangle_{\mathrm{Al}}$ is quite similar to that of the ^{57}Fe average centre shift $\langle\delta\rangle$: slow variations are observed for samples along the I-, M-, and A-lines, whereas larger changes are observed when going from one domain to another. As demonstrated in section 4.2.1, the changes of $\langle\delta\nu\rangle_{\mathrm{Al}}$ *reflect changes in the electronic properties only*. To a first approximation, the different NMR central lines are simply shifted while their linewidths remain nearly the same, as can be seen for example in figure 6. In conclusion, the variations of $\langle\delta\nu\rangle_{\mathrm{Al}}$ from sample to sample reveal homogeneous changes in the electronic couplings at the Al sites. Moreover, the local electronic properties depend on the composition in a similar way at the Al and Fe sites. Note that, whereas the average quadrupole splitting at the Fe site varies with the average centre shift, no changes in the EFG distribution at the Al sites could be detected within experimental accuracy.

4.3.2. Cu sites. The average frequency shift $\langle\delta\nu\rangle_{\mathrm{Cu}}$ increases from the I- to the M-line, and from the M-line to the A-line (see figure 3(d)). No clear evolution is observed along either line, but changes may be masked by the large error bars. As discussed in section 4.2.2, these changes must reflect mainly some variations in the electronic properties, the EFG distribution remaining approximately the same. These variations of $\langle\delta\nu\rangle_{\mathrm{Cu}}$ are accompanied by large changes in the linewidth as can be seen in figure 3(e). Therefore, contrary to the Al case, no global shift of the ^{65}Cu central lines in 7 T occurs from sample to sample. The evolution of the ^{65}Cu resonance with the Cu composition along the A-line could indeed suggest that additional Cu sites are occupied with increasing Cu content. These new sites would then correspond to larger frequency shifts (see figure 6). In conclusion, although clear changes in the electronic properties at the Cu sites occur, they are more difficult to interpret than those at the Fe and Al sites, presumably because of simultaneous chemical changes (site occupation).

4.4. Correlation between the hyperfine properties at Fe and Al sites

Due to the observed similarity between the composition dependence of the ^{27}Al average frequency shift $\langle\delta\nu\rangle_{\mathrm{Al}}$ measured in 7 T and of the ^{57}Fe average centre shift $\langle\delta\rangle$, the possibility of the existence of a correlated variation of these two quantities, such as the one discussed in section 3.3, must be examined. Indeed, when plotting $\langle\delta\nu_{\mathrm{e}}\rangle_{\mathrm{Al}}$ as a function of $\langle\delta\rangle$ (figure 8) a clear correlation is found for all samples on the I-, A-, and M-lines. (Because of the linear $\langle\Delta\rangle$–$\langle\delta\rangle$ relation, $\langle\Delta\rangle$ could have been used instead.) The correlation line is given by

$$\langle\delta\nu_{\mathrm{e}}\rangle_{\mathrm{Al}} = -231\langle\delta\rangle + 67\ \mathrm{kHz}. \tag{2}$$

This behaviour demonstrates the existence of *correlated changes in the local electronic properties with composition at the Al and Fe sites in icosahedral and high-order approximant phases*. No detectable correlation exists with the EFG distribution at the Al sites which was found to be constant within the accuracy of the experiment. Just as in the case of the correlation between $\langle\delta\rangle$ and $\langle\Delta\rangle$, the results for sample i-(26, 12.2) fall on the correlation line described by equation (2). The results for the low-order cubic approximant fall rather close to the correlation line, in contradistinction to the results for the iron EFG–isomer shift correlation shown in figure 5. The average shifts for the crystalline non-approximant phases are not presented here because they are all very different from those for the QC and approximants. No similar analysis can be performed to link the variations of $\langle\delta\nu\rangle_{\mathrm{Cu}}$ with those of other properties

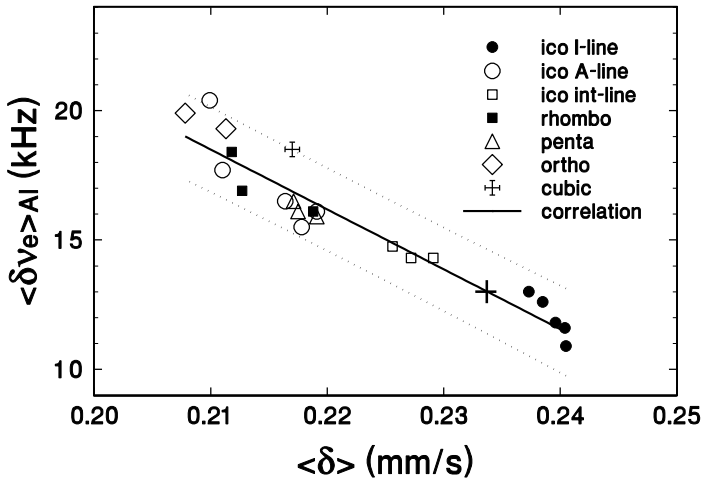

Figure 8. A correlation diagram showing the linear dependence between the ^{57}Fe centre shift $\langle\delta\rangle$ and the ^{27}Al NMR frequency shift $\langle\delta\nu_e\rangle_{Al}$ at 6.9952 T for samples along the I-, A-, and M-lines. The sample marked + is the additional i-phase i-(26.0, 12.2) discussed in the text. The solid line is a fit to the data and the dotted lines are the 95% confidence limits.

because this parameter does not reflect the global changes in the electronic properties alone (see section 4.3.2).

5. Analysis of results

We have shown that changes in several of the ^{57}Fe and ^{27}Al nuclear hyperfine properties are correlated with each other. This is the case for the ^{57}Fe Mössbauer centre shift $\langle\delta\rangle$ and quadrupole splitting $\langle\Delta\rangle$, and the NMR average *electronic* shift $\langle\delta\nu_e\rangle$ for ^{27}Al. We now want to discuss the meaning of these results for the understanding of the local electronic structure in the phases found in the icosahedral and high-order approximant stability regions of the ternary phase diagram.

5.1. Correlations on the iron site

Such correlations in the hyperfine properties on one single nuclear site are well known in the literature on Mössbauer spectroscopy. Covalent compounds containing tin, gold, antimony or tellurium have long been studied, and many cases of $\langle\delta\rangle$–$\langle\Delta\rangle$ correlations have been found (see for instance references [29, 30]). The Mössbauer isomer shift δ is given by [30]

$$\delta = \frac{4\pi}{5} Z e^2 S' \bar{R}^2 \frac{\Delta R}{R} (\langle|\Psi(0)|^2\rangle_A - \langle|\Psi(0)|^2\rangle_S). \tag{3}$$

In this expression, Z is the atomic number, e the electronic charge, $\bar{R}$ the average nuclear radius, and $\Delta R/R$ the relative change in radius between excited and ground states. S' is a relativistic correction. The s-electron density averaged over the (small) volume of the nucleus is denoted as $\langle|\Psi(0)|^2\rangle_X$, where X = A is the absorber, and X = S the source.

We can express the electric quadrupole splitting as [30]

$$\Delta = \left|\frac{1}{2} e^2 q Q\right| \sqrt{1 + \eta^2/3} \tag{4}$$

where q is the absolute largest principal component of the EFG tensor: $eq = eq_{zz} = \partial^2 V/\partial z^2$ (V being the electrostatic potential at the nucleus). Q is the nuclear quadrupole moment. The asymmetry parameter is given by $\eta = (q_{xx} - q_{yy})/q_{zz}$, and, as usual, $0 \leqslant \eta \leqslant 1$ as long as we choose $|q_{zz}| \geqslant |q_{yy}| \geqslant |q_{xx}|$. The EFG arises from the non-spherical charge distribution around the nucleus, but it is now well known that it is dominated by the partially filled valence p and d orbitals of the atom itself [31]. The largest EFG effects are seen in covalent compounds with unequal populations in the p_x, p_y, and p_z orbitals. Thus 3p orbitals will dominate the EFG if they are partially filled. In the case of Fe, we expect mainly a 3d–4s character at the Fermi surface with some 4p contribution, and an EFG dominated by 3d and 4p orbitals.

In addition to the direct contributions of the s orbitals to the isomer shift, and the unfilled p and d orbitals to the EFG tensor, there are also *indirect* contributions to these properties. This is due to changes in the density of the s orbitals, as well as the average $\langle r^{-3}\rangle$ of the p and d orbitals with the occupations of the other orbitals. De Vries *et al* [32] have given the results of numerical relativistic self-consistent calculations of the s-electron density at the nucleus $\langle|\Psi(0)|^2\rangle$ and $\langle r^{-3}\rangle$ for the case of Fe atoms. They give the following expressions:

$$\langle|\Psi(0)|^2\rangle = \rho_0 + An_s - Bn_p - C(n_d - 5) - Dn_s(n - 5) \tag{5}$$

$$\langle r^{-3}\rangle_d = \langle r^{-3}\rangle_0 - E(n_d - 5) - Fn_s - Gn_p. \tag{6}$$

Here, $n = n_s + n_p + n_d$, the number of 'valence' (3d, 4s, 4p) electrons. The constants ρ_0 and $\langle r^{-3}\rangle_0$ give the values for the $3d^5 4s^0 4p^0$ state. The numerical constants A to G are given for iron in table 2, as taken from [32]. (The constants in equation (6) depend on m, but this dependence is very weak and will be ignored here.) Their ideas were applied to a series of different gold compounds, using the ^{197}Au Mössbauer isomer shift and EFG splitting, by Viegers and Trooster [33, 34]. Such compounds show a linear correlation between Δ and δ for compounds of the same symmetry but for different covalence (due to a different electronegativity of neighbouring atoms). Since the isomer shift is proportional to $\langle|\Psi(0)|^2\rangle$, and the magnitude of the EFG tensor is proportional to $\langle r^{-3}\rangle_{p,d}$, we expect such a correlation on one nuclear site with systematic (and continuous) changes in covalency (orbital occupation) but only as long as the basic structure (or building blocks) does not change. The calculation of de Vries *et al* is only correct for isolated atoms, and is questionable for the case of a metal with delocalized electron states forming bands. However, we will use it to make a rough estimation of the correlation effect at the iron site. More detailed calculations are very difficult even for simple structures, especially for the case of the iron EFG, dominated by *both* p and d orbitals.

Table 2. Values given by de Vries *et al* [32] (see the text).

A	*B*	*C*	*D*	*E*	*F*	*G*
13.86	0.03	3.48	2.25	0.63	0.13	0.10

From the signs of the different terms given above (which differ for n_s- as compared to n_p- and n_d-contributions) we can conclude that the slope of the correlation diagram is consistent with a continuous variation in mainly the p- and d-orbital occupations on the iron atoms. Higher occupations of these orbitals lead to an increase in the isomer shift and a decrease in the EFG splitting (for ^{57}Fe, the isomer-shift calibration constant is negative). We conclude that the stable and metastable icosahedral quasicrystals and high-order approximant phases build a continuous series characterized by changes in the p- and d-orbital occupations on iron [35]. The negative slope of the correlation line corresponds to larger values of the quadrupole splitting for larger $\langle|\Psi(0)|^2\rangle$. The perfect icosahedral samples along the I-line show the smallest values of these parameters, which would correspond to the largest values of p- and d-orbital occupation.

We now estimate the slope $\partial\Delta/\partial\delta$. If we take the simple example of a d^6 configuration in a distorted octahedral field, then the EFG q varies from $-(2/7)\langle r^{-3}\rangle$ to $(4/7)\langle r^{-3}\rangle$ [30]. In the following, we take an average coefficient of 3/7, and assume that there is one electron contributing to Δ. In order to estimate the magnitude of the changes produced in δ and Δ, we calculate the variations with respect to the d-orbital occupancy. From this, using the numerical coefficients found in de Vries *et al* [32], we find

$$\frac{\partial\Delta}{\partial\delta} \approx -1.3\frac{\partial\langle r^{-3}\rangle}{\partial\langle|\Psi(0)|^2\rangle} \approx -1.3\frac{E+G-F}{C+B-D(n-5)} \approx -1.3\frac{E}{C} \approx -0.2 \qquad (7)$$

while the experimental coefficient found above is -2.2. Thus we can conclude that this very simple estimation gives the correct sign of the changes observed (but is very sensitive to the value of $n-5\approx 0$ chosen). Our estimation only involves one d-orbital contribution to q, and neglects the important 3p and 4p contributions on Fe. This leads to our underestimation of the magnitude of the slope.

In this discussion of the hyperfine properties of ^{57}Fe we have used a chemical model assuming covalent bonds between iron and its neighbours. As discussed below, AlCuFe QCs are metallic, so our approach is only a zeroth-order model. Our goal is to give an idea of the contributions leading to the correlation on iron, and not an exact description.

5.2. Correlation between the ^{57}Fe isomer shift and the ^{27}Al electronic shift

In order to discuss this correlation, we first have to discuss the origin of the ^{27}Al NMR line shift. We first note that the measured average shifts shown in table 1 and figure 3 are small, and that they remain small even after correcting for the quadrupole shift, as discussed above. The relative shifts $K=\delta\nu_e/\nu_L$ are in the range 0.13×10^{-3} to 0.26×10^{-3}, i.e. about 10 to 20% of the shift measured in metallic Al, $K=1.64\times10^{-3}$ [36, 37].

In a metal, the shift of the ^{27}Al NMR line results from the interaction of the nucleus with conduction electrons. Usually the dominant contribution is due to from the contact interaction between the nucleus and the s part of the conduction electron wavefunction. The corresponding Knight shift K_s is equal to $(8\pi/3)\chi_P\langle|\Psi(0)^2|\rangle_{FS}$. The Pauli susceptibility of the electron gas per atom is given by $\chi_P=\mu_B^2N(E_F)$, and $\langle|\Psi(0)^2|\rangle_{FS}$ is the density of s electrons at the nucleus just as in the case of the isomer shift, but in this case averaged over the Fermi surface. In addition to the contact interaction, indirect couplings of the nucleus with the p and d parts of the conduction electron wavefunction occur through the induced polarization of the inner 1s and 2s core states. In the case of metallic Al, a complete calculation of these core terms has been performed [37]. The results of this calculation are that the coupling of inner core states with the p conduction states averages to zero, while the coupling with d conduction states leads to a small negative shift. The coupling of s conduction states with core s states also leads to a small positive shift which provides a small correction (less than 10%) of the direct contact interaction. There is also an orbital contribution which in the case of aluminium metal is negligible [37].

The high resistivity of QCs raises the question of the validity of treating the NMR shift as a metallic shift. Indeed band-structure calculations of approximant phases reveal also that the spatial extent of the electronic states at the Fermi level follows a power law [38]. However, in AlCuFe QCs, the electronic density of states (DOS) at the Fermi level is reduced but is *non-zero*. The electronic contribution to the specific heat is found to be about a third of that found for metallic aluminium [39]. Using these data to estimate χ_P in a crude approximation, one would expect a reduction by at least a factor of 3 of the shift, compared to that of metallic Al. In addition, the wavefunctions at the Al site in quasicrystals and approximants are strongly

affected by the hybridization with Cu and Fe conduction states. Numerical calculations of the local conduction bands in model quasicrystals [40] have shown a small but definite occupation of Al-centred d orbitals. Thus, we expect for ^{27}Al in AlCuFe a negative core contribution in addition to the positive K_s, which would reduce the measured relative shift K. This contribution could very well explain our results and especially their sensitivity to small composition variations. If K varies, then the nuclear spin–lattice relaxation time T_1 should also change. We have studied the nuclear relaxation at 80 K in several samples along the I- and A-lines. No differences were found within experimental accuracy. However, different contributions to T_1 are additive, so this parameter is much less sensitive than K to the changes in s and d character of the wavefuctions at the Fermi level. (In addition, it remains unclear whether the nuclear spin relaxation is dominated by couplings with the conduction electrons, or by atomic movements which modulate quadrupole couplings.)

If the results obtained for metallic Al can be carried over to quasicrystals and approximants, the contribution of p-electron conduction states to the shift is nearly negligible. In contrast, the EFG measured for ^{27}Al should be dominated by the contribution from the 3p orbitals (plus a small contribution due to 3d orbitals). As we have discussed in section 4.2.1 and shown in figure 7, the EFG quadrupole shift distribution remains constant over all the icosahedral and high-order approximant samples. This is a very strong argument for a constant p-orbital occupation on Al over these different compositions and structures. The small d-orbital variations proposed to explain the changes in the electronic shifts are too small to be seen in the EFG in the presence of the (relatively large) electric field gradient of the p orbitals. (Contributions to the EFG vary as $\langle 1/r^3 \rangle$, and this is much larger for p than d orbitals.)

In conclusion, in order to explain the changes in the Knight shift while the quadrupole interaction remains constant, the occupations of the p states can be assumed constant while the s and d occupations vary. In this case, the correlation of the aluminium $\langle \delta\nu \rangle_e$ and the iron Mössbauer average centre shift $\langle \delta \rangle$ can be ascribed to simultaneous changes in the occupation of s and induced d orbitals on Al, and p and d orbitals on Fe atoms in the AlCuFe structure.

6. Discussion

We have presented a detailed study of the hyperfine properties at the Fe, Al, and Cu sites in quasicrystalline AlCuFe and approximants. Our goal was to elucidate details of the *local chemical and electronic structure* which contribute to the stability of these phases. The main observations and conclusions are discussed below.

The small variations in the hyperfine properties of ^{57}Fe and ^{27}Al along and in between the composition lines show some inter- and intra-nuclear correlations. That is, there are uniform changes in these properties over the whole composition range of the stable phases. The changes are correlated between iron (average isomer shift and EFG) and aluminium (average electronic shift), but not for copper or for the EFG of aluminium. The simplest interpretation of these correlations is based on the changes in covalent bonding with composition resulting in changes in orbital occupations for Fe and Al. This leads us to a model where there is strong overlap between Fe p and d orbitals, and the d orbitals induced on Al. The fact that all QC and high-order approximant samples are described by the same correlations shows that there is a systematic variation of the hybridization of d orbitals on Al, and p and d orbitals on Fe over the composition range. *These correlations thus unify the different stable concentration domains otherwise characterized by different values of e/a in a Hume-Rothery approach* (see figure 1). Therefore we can conclude that the local hybridization (between Al and Fe atoms) is important in determining the structural stability of QC and approximant phases.

The importance of hybridization between iron d states and aluminium sp conduction

states has already been shown by extensive experimental and numerical studies of the electronic band properties of AlCu and AlCuFe alloys [41, 42]. The comparison of binary AlCu Hume-Rothery alloys with AlCuFe QC shows that the Fe d states repel the conduction Al sp states away from the Fermi level, thus increasing the pseudo-gap [43]. This is also the reason for the seemingly strange Hume-Rothery iron valence of -2 used to describe the stability domains in the phase diagram. This effect had been predicted by analytical models and is also clear from band-structure calculations which show strong sp–d hybridization effects [14, 40].

In the light of these new results on the local electronic properties in the AlCuFe QC and approximant phases, it is interesting to discuss previous studies of the composition dependence of the electronic properties.

The specific heat $C_v(T)$ of AlCuFe has been studied by several different groups [39]. These results have been analysed in terms of a linear electronic and cubic (and higher) lattice contributions at low temperatures. The coefficient of the linear term is the electronic Sommerfeld coefficient γ, which is usually found to be of the order of 0.3 mJ mol^{-1} K^{-2} (but with large errors). This leads to the expectation that the density of states at the Fermi level should be about one third of that in metallic aluminium. There are however not enough data in the literature to judge whether there is any dependence on concentration or number of conduction electrons e/a as found for the hyperfine properties presented here.

The electrical resistivity $\rho(T)$ is found to be very high [44,45]. It is also found to depend on sample quality and that the resistivity *increases* with increasing structural perfection, contrary to the case for good metals. This high resistivity has been commonly attributed to the pseudo-gap at the Fermi energy and a reduced mobility [10, 46]. Except for those given by Lindqvist *et al* [45] the data presented in the literature are only for a restricted composition range, so it is not possible to discuss these as a function of composition or of the number of conduction electrons e/a. The results of Lindqvist *et al* show that there is no scaling of the conductivity σ or the Hall coefficient R_{H} at 4 K with e/a, but rather with the iron concentration.

The magnetic susceptibility is found to be diamagnetic [44, 47]. This again shows the strong deviation from 'good-metal' properties and the reduction in the density of states at the Fermi level in these quasicrystals and high-order approximants. There are no systematic changes from sample to sample (composition, e/a) within experimental accuracy [48].

Soft x-ray emission and photoabsorption spectroscopies give an indication of the variation of the band structure in the neighbourhood of the Fermi level. Belin *et al* [42] have followed the variations in the Al 3s and 3p, the Cu 3d–4s, and the Fe 3d–4s states for icosahedral, decagonal, and conventional crystalline samples in AlCuFe(Cr) alloys. Their general conclusion is that there is a strong reduction in the density of states at the Fermi level. In addition, the maxima of the states move away from E_{F} by about 3/4 eV. These observations are consistent with the presence of a pseudo-gap at E_{F} and a density of states of $N(E_{\mathrm{F}})$ of about 30% of that in pure Al metal for the icosahedral and decagonal samples. However, due to the relatively low resolution of this method, there is no possibility of seeing small changes with composition.

Thus the great advantage of hyperfine methods is their relatively high sensitivity to small changes in electronic properties which we have seen to occur in the i-AlCuFe QC and approximant system with composition.

7. Conclusions

We have presented studies of the local electronic properties and the atomic order in $Al_{100-x-y}Cu_xFe_y$ phases using ^{57}Fe Mössbauer, and ^{27}Al and ^{65}Cu NMR spectroscopies. Our main findings are the following. The ^{57}Fe Mössbauer quadrupole splitting is linearly related to the centre shift (isomer shift) for all samples, which reveals systematic changes in the

orbital occupations on Fe atoms with composition. It is also found that the ^{27}Al NMR average electronic shift follows this correlation. The results are described in terms of the systematic changes in covalence caused by the hybridization between orbitals on Fe and Al. This leads us to a model where there is strong overlap between Fe p and d orbitals and the d orbitals induced on Al. We have studied also a low-order cubic approximant phase containing Si as well as several crystalline phases: these results do not fall on the correlation line, indicating different atomic binding.

Acknowledgments

The research was supported in part by the German–French DAAD–APAPE Procope programme, as well as by the DFG Focus Programme 'Quasikristalle: Struktur und physikalische Eigenschaften'. Part of this work was performed during the visit of one of the authors (RAB) to the Laboratoire de Physique des Solides, Université de Paris Sud, with the support of the CNRS.

Appendix. Fits of the NMR lines

In order to better characterize the EFG distribution at the Al and Cu sites and separate the electronic and quadrupole contributions to the central-line position, we have undertaken simulations of the NMR lines. We have followed a procedure very close to that detailed in reference [26]. We considered only the case where the quadrupolar Hamiltonian H_q can be treated as a perturbation of the Zeeman part and we neglected the coupling of nuclei with the electrons H_e. In order to compute the powder averaged pattern, a hypothesis as regards the distributions of the EFG tensor parameters q ($eq = \partial^2 V/\partial z^2$) and of the asymmetry parameter η is needed. We assumed

$$f(q,\eta) = \frac{q^4\eta}{\sqrt{2\pi}\sigma^5}\left(1-\frac{\eta^2}{9}\right)\exp\left[-\frac{q^2}{2\sigma^2}\left(1+\frac{\eta^2}{3}\right)\right]. \tag{A.1}$$

This model, called the Gaussian isotropic model (GIM), applies to a large number of cases and not only to the case of an EFG tensor based on a point-charge model in the presence of a random distribution of electric charges [20]. It will also be true for long-ranged oscillating potentials, as encountered in aluminium-based (Al)–transition metal (TM) amorphous [20] or quasicrystalline solids where strong and long-range interactions between Al and TM play an important role [49]. Indeed it has been shown in [15] that this model fits the ^{57}Fe Mössbauer spectra for AlCuFe QC and approximants well, so it seems natural to try to apply it to describe the NMR spectra. It should be emphasized that the GIM probability is entirely defined by *one single* parameter σ, or alternatively the average $\langle|q|\rangle = 1.9947\sigma$. (Both our NMR and Mössbauer studies are only sensitive to the absolute value of q.) For fitting the NMR lines we introduced $\nu_q = 3e^2|qQ|/(2I(2I-1)h)$ (with Q the nuclear quadrupole moment and I the nuclear spin) [50].

A very good description of the ^{27}Al NMR satellite spectra measured for the sample i-(25.5, 12.5) can be obtained within the GIM model with $\langle\nu_q\rangle = 1.6$ MHz as can be seen in figure 7(a). The central line, measured at a frequency (18 MHz) low enough that it is dominated by quadrupole effects only, can also be fitted with the same $\langle\nu_q\rangle$ value. For ^{65}Cu the central line measured at 40.454 MHz can also be described in the GIM model with $\langle\nu_q\rangle = 4.4$ MHz (see figure 7(b)). The argument is not as good as in the case of Al at 18 MHz because for Cu at 26 MHz, about 20% of the width is not of quadrupolar origin. Unfortunately data at lower frequency are not reliable enough to permit the use of a fitting procedure.

The GIM model is only slightly different from the model used by Shastri *et al* in reference [26] who assumed $f(q,\eta) = G(|q|)F(\eta)$ where $G(|q|)$ is a Gaussian function centred on $\langle|q|\rangle$ (standard deviation σ_G) and F was taken as constant over a given range of η. In the GIM model the marginal distribution of $|q|$ is not far from a Gaussian, with a mean square-root deviation equal to $0.325\langle|q|\rangle$. However, the marginal distribution of η is far from being flat and $\eta = 0$ has a zero probability. We also tried to analyse our data using the hypothesis of reference [26]. These fits were not as good as those obtained from the GIM model. Details of these fits will be published elsewhere. Note that the difference between the $\langle\delta\nu_q\rangle$ values at Al and Cu sites mainly reflects the different nuclear angular momentum values and that the $\langle|q|\rangle$ values deduced are very similar. For ^{27}Al, using $\langle\delta\nu_q\rangle = 1.6$ MHz and $Q = 0.15$ b, we obtain $\langle|V_{zz}|\rangle = 3.0$ V m^{-2}. For ^{65}Cu, using $\langle\delta\nu_q\rangle = 1.6$ MHz and $Q = -0.15$ b, we obtain $\langle|V_{zz}|\rangle = 2.4$ V m^{-2}.

In conclusion, good fits of the NMR spectra for i-(25.5, 12.5) could be obtained in the framework of the GIM model. Due to the similarity of the NMR spectra measured for all QC and high-order approximant phases, the same conclusions are valid for all samples studied. Quasicrystals and high-order approximants are therefore characterized by a large distribution of local environments whose consequences for the NMR lines are indistinguishable from those of a random distribution of the EFG. However, as shown in reference [20] a small amount of disorder may be sufficient to reach the validity domain of the GIM equation.

We can now compare the average EFG at Al and Cu sites with that for Fe (in all cases for the i-(25.5, 12.5) sample). At the ^{57}Fe site, $eq_{zz} = V_{zz}$ can be simply deduced from $\langle\Delta\rangle$ using equation (4). In the GIM model, $\langle\Delta\rangle = (1/2)|eQ|\langle|V_{zz}|\rangle\sqrt{1+\eta^2/3}$ (with $\eta \approx 0.6$). Then, from $\Delta = 0.38$ mm s^{-1}, we obtain $\langle|V_{zz}|\rangle = 2.2$ V m^{-2} using $Q = 0.16$ b [51]. It is striking that we see quite similar values of the average EFG interaction at all three sites, despite large differences in local configurations expected from the current structural models [7,8]. However, a detailed analysis of these results would go beyond our knowledge of the details of the EFG interactions in this material and would be rather speculative.

Once $\langle\nu_q\rangle$ has been determined, the average quadrupole shift of the central line, $\langle\delta\nu_q\rangle$, can be computed analytically. For a given ν_q and η, one can calculate [50]

$$\langle\delta\nu_q\rangle = -\nu_q^2(I(I+1) - 3/4)(1+\eta^2/3)/(30\nu_L).$$

In the GIM model the average of $(1+\eta^2/3)\nu_q^2$ over ν_q and η is equal to $5\sigma^2$ (or $5\langle\nu_q\rangle^2/4$). Then, for the final spectrum,

$$\langle\delta\nu_q\rangle = -\langle\nu_q\rangle^2(I(I+1) - 3/4)/(24\nu_L).$$

From the fits discussed above, one obtains -11 kHz for ^{27}Al (-29 kHz for ^{65}Cu) in 6.9952 T. For the ^{27}Al resonance, this value was used to correct the measured shifts $\langle\delta\nu\rangle_{Al}$ and obtain the electronic contribution to the shift (sections 4.4 and 5.2).

References

[1] Shechtman D, Blech I, Gratias D and Cahn J W 1984 *Phys. Rev. Lett.* **53** 1951

[2] Janot Ch and Mosseri R (ed) 1995 *Proc. 5th Int. Conf. on Quasicrystals* (Singapore: World Scientific)

[3] Hippert F and Gratias D (ed) 1994 *Lectures on Quasicrystals* (Paris: Les Editions de Physique)

[4] Takeuchi S and Fujiwara T (ed) 1998 *Proc. 6th Int. Conf. on Quasicrystals* (Singapore: World Scientific)

[5] See, for example,
Duneau M 1994 *Lectures on Quasicrystals* ed F Hippert and D Gratias (Paris: Les Editions de Physique) ch 2, pp 153–86

[6] Cornier-Quiquandon M, Quivy A, Lefebvre S, Elkaim E, Heger G, Katz A and Gratias D 1991 *Phys. Rev.* B **44** 2071

[7] Katz A and Gratias D 1995 *Proc. 5th Int. Conf. on Quasicrystals* ed Ch Janot and R Mosseri (Singapore: World Scientific) p 164
[8] Stephens P W and Goldman A I 1986 *Phys. Rev. Lett.* **56** 1168
Stephens P W and Goldman A I 1986 *Phys. Rev. Lett.* **57** 2331 (erratum)
Stephens P W and Goldman A I 1986 *Phys. Rev. Lett.* **57** 2770
[9] Poon S J 1992 *Adv. Phys.* **41** 303
[10] Mayou D 1994 *Lectures on Quasicrystals* ed F Hippert and D Gratias (Paris: Les Editions de Physique) ch 9, pp 417–62
Berger C 1994 *Lectures on Quasicrystals* ed F Hippert and D Gratias (Paris: Les Editions de Physique) ch 10, pp 463–504
[11] Janot Ch and Mosseri R (ed) 1995 *Proc. 5th Int. Conf. on Quasicrystals* (Singapore: World Scientific) ch 4
[12] Hume-Rothery W and Raynor G V 1954 *The Structure of Metals and Alloys* (London: Institute of Metals)
[13] Quiquandon M, Quivy A, Devaud J, Faudot F, Lefebvre S, Bessière M and Calvayrac Y 1996 *J. Phys.: Condens. Matter* **8** 2487
[14] Trambly de Laissardière G, Mayou D and Nguyen Manh D 1993 *Europhys. Lett.* **21** 25
Trambly de Laissardière G, Nguyen Manh D, Magaud L, Julien J P, Cyrot-Lackmann F and Mayou D 1995 *Phys. Rev.* B **52** 7920
[15] Hippert F, Brand R A, Pelloth J and Calvayrac Y 1994 *J. Phys.: Condens. Matter* **6** 11 189
[16] Hippert F, Brand R A, Pelloth J and Calvayrac Y 1995 *Proc. 5th Int. Conf. on Quasicrystals* ed Ch Janot and R Mosseri (Singapore: World Scientific) pp 464–71
[17] Quivy A, Quiquandon M, Calvayrac Y, Faudot F, Gratias D, Berger C, Brand R A, Simonet V and Hippert F 1996 *J. Phys.: Condens. Matter* **8** 4223
[18] Sâadi N, Faudot F, Gratias D and Legendre B 1995 *Proc. 5th Int. Conf. on Quasicrystals* ed Ch Janot and R Mosseri (Singapore: World Scientific) pp 656–59
Quiquandon M, Quivy A, Faudot F, Sâadi N, Calvayrac Y, Lefebvre S and Bessière M 1995 *Proc. 5th Int. Conf. on Quasicrystals* ed Ch Janot and R Mosseri (Singapore: World Scientific) pp 152–5
[19] Black P J 1955 *Acta Crystallogr.* **8** 43
Black P J 1955 *Acta Crystallogr.* **8** 175
[20] Le Caër G and Brand R A 1999 *J. Phys.: Condens. Matter* **10** 10 715
[21] Faudot F 1993 *Ann. Chim.* **18** 445
[22] Freiburg C and Grushko B 1994 *J. Alloys Compounds* **210** 149
[23] Hippert F, Brand R A, Pelloth J and Calvayrac Y 1998 *Aperiodic '97* ed M de Boissieu and J-L Verger-Gaugry (Singapore: World Scientific) p 745
[24] Lawther D W and Dunlap R A 1993 *J. Non-Cryst. Solids* **153+154** 45
[25] Van der Kraan A M and Buschow K H J 1986 *Physica* B **136** 55
[26] Shastri A, Borsa F, Torgeson D R, Shield J E and Goldman A I 1994 *Phys. Rev.* B **50** 15 651
[27] This background can be taken as constant under the ^{27}Al central line but it decreases with increasing frequency under the ^{65}Cu central line because of the contribution of the ^{27}Al first-order quadrupole line.
[28] Comparisons between different samples at lower frequencies, where quadrupole effects are dominant, are not accurate enough, because the ^{65}Cu central line becomes broader and separating it from the Al contribution becomes more and more difficult.
[29] Parrish R V 1984 *Mössbauer Spectroscopy Applied to Inorganic Chemistry* vol 1, ed G J Long (New York: Plenum) pp 527–76, 577–618
[30] Vértes A, Korecz L and Burger K 1979 *Mössbauer Spectroscopy* (Amsterdam: Elsevier Scientific)
[31] Blaha P, Schwarz K and Dederichs P H 1988 *Phys. Rev.* B **37** 2792
[32] de Vries J L F K, Trooster J M and Ros P 1975 *J. Chem. Phys.* **63** 5256
[33] Viegers P M A 1976 *PhD Thesis* Katholieke Universiteit te Nijmegen
[34] Viegers P M A and Trooster J M 1978 *Hyperfine Interact.* **4** 813
[35] In addition, we also expect the asymmetry seen within one spectrum not to be related to the correlation between spectra. This is because the first describes shifts in the local δ and Δ between different local configurations at fixed composition, while the second, and new, correlation describes the slight shifts in covalence with the overall composition for each local configuration.
[36] Carter G C, Bennet L H and Kahan D J 1977 *Metallic Shifts in NMR* (Oxford: Pergamon)
[37] Shyu W-M, Das T P and Gaspari G D 1966 *Phys. Rev.* **152** 270
[38] Fujiwara T, Mitsui T and Yamamoto S 1996 *Phys. Rev.* B **53** R2910
[39] Wang K, Scheidt C, Garoche P and Calvayrac Y 1992 *J. Physique* **2** 1553
Pierce F S, Bancel P A, Biggs B D, Guo Q and Poon S J 1993 *Phys. Rev.* B **47** 5670
Lasjaunias J C, Calvayrac Y and Yang Hongshun 1997 *J. Physique* I **7** 959

[40] Trambly de Laissardière G and Fujiwara T 1994 *Phys. Rev.* B **50** 5999
[41] Trambly de Laissardière G, Dankházi Z, Belin E, Sadoc A, Nguyen Manh D, Mayou D, Keegan M and Papaconstantopoulos D 1995 *Phys. Rev.* B **51** 14 035
[42] Belin E, Dankházi Z, Sadoc A, Dubois J M and Calvayrac Y 1994 *Europhys. Lett.* **26** 677
[43] Fournée V, Belin-Ferré E and Dubois J M 1998 *J. Phys.: Condens. Matter* **10** 4231
Belin-Ferré E, Fournée V, Dubois J M and Sadoc A 1998 *Proc. 6th Int. Conf. on Quasicrystals* ed S Takeuchi and T Fujiwara (Singapore: World Scientific) p 603
[44] Mayou D, Berger C, Cyrot-Lackmann F, Klein T and Lanco P 1993 *Phys. Rev. Lett.* **70** 3915
Klein T, Berger C, Mayou D and Cyrot-Lackmann F 1991 *Phys. Rev. Lett.* **66** 2907
[45] Lindqvist P, Berger C, Klein T, Lanco P, Cyrot-Lackmann F and Calvayrac Y 1993 *Phys. Rev.* B **48** 630
[46] Mizutani U 1998 *J. Phys.: Condens. Matter* **10** 4609
[47] Matsuo S, Nakano H, Ishimasa T and Fukano Y 1989 *J. Phys.: Condens. Matter* **1** 6893
[48] Hippert F, Brand R A and Calvayrac Y, to be published
[49] Zou J and Carlsson A E 1994 *Phys. Rev.* B **50** 99
[50] Cohen M H and Reif R 1957 *Solid State Physics* vol 5, ed F Seitz and D Turnbull (New York: Academic) p 321
[51] Dufek P, Blaha P and Schwarz K 1995 *Phys. Rev. Lett.* **75** 3545